Formate Adsorption on the (111) Surface of Rutile TiO_2

Hiroshi Uetsuka,[†,§] Michael A. Henderson,[‡] Akira Sasahara,[†,⊥] and Hiroshi Onishi*[,†,⊥]

Surface Chemistry Laboratory, Kanagawa Academy of Science and Technology, KSP, Sakado, Takatsu, Kawasaki, 213-0012 Japan, and Interfacial Chemistry and Engineering Group, Pacific Northwest National Laboratory, Richland, Washington 99352

Received: February 27, 2004; In Final Form: June 11, 2004

The (111) surface of rutile TiO_2 was prepared with argon ion sputtering and vacuum annealing at 970 K. Scanning tunneling microscope observation revealed nanometer-scale domains of (1×1) and (1×2) phases on the surface. Formic acid was dissociatively adsorbed on the surface at room temperature. The recombination and decomposition temperatures of the adsorbed formate were similar to those reported on the (110) surface. The CH-related and COO-related stretching modes probed by high-resolution electron energy loss showed two or more types of formate. The wavenumber of the vibrational modes can be interpreted with a mixture of monodentate, bidentate, and bridge form of adsorption. The number density of the formates counted in microscope images supported monodentate and bidentate forms. Sequential imaging revealed limited mobility of the formates, reflecting the wide separation of surface Ti atoms.

1. Introduction

Chemistry on well-defined surfaces of TiO_2 has been developed in recent years.[1−7] Single crystalline surfaces of rutile (110),[8] (100),[9] (001),[10] and (111)[11] and anatase (001),[12] (101),[13] and (100)[14] are prepared in an ultrahigh vacuum. Formate, a simple organic anion, is used to probe chemical properties on these surfaces.[15] Formic acid is dissociatively adsorbed to give a formate and a proton. Topmost Ti atoms make a row on the rutile (110) surface with the Ti−Ti distance of 296 pm along the row axis. The formate is bridge-adsorbed on two Ti atoms with its O−C−O plane parallel to the row. Photoelectron diffraction,[16] vibrational spectroscopy,[17,18] electron-stimulated desorption,[19] X-ray absorption,[20] scanning tunneling microscope,[21] noncontact atomic force microscope,[22] and theoretical[23] studies evidenced the bridge form of adsorption. The O−O distance of a formate (ca. 0.25 nm) is close to the Ti−Ti distance and favors the bridge adsorption.

In the present study, the formate is adsorbed on the (111) surface which provides the largest Ti−Ti distance among low-index planes of rutile. Figure 1 illustrates an ideal structure of the stoichiometric (111) surface, where the coordination with topmost Ti and O atoms is optimized to be 5-fold and 2-fold, respectively.[11] The nearest Ti−Ti distance (546 pm) is much larger than the O−O distance of a formate which makes the bridge adsorption unfavorable. It is examined what type of formate coordination (bridge, bidentate, or monodentate) is available on this surface. Evidence for bidentate and monodentate coordination is provided. The reactivity and mobility of such coordinated species are compared with those of the bridge formate prepared on the (110) surface.

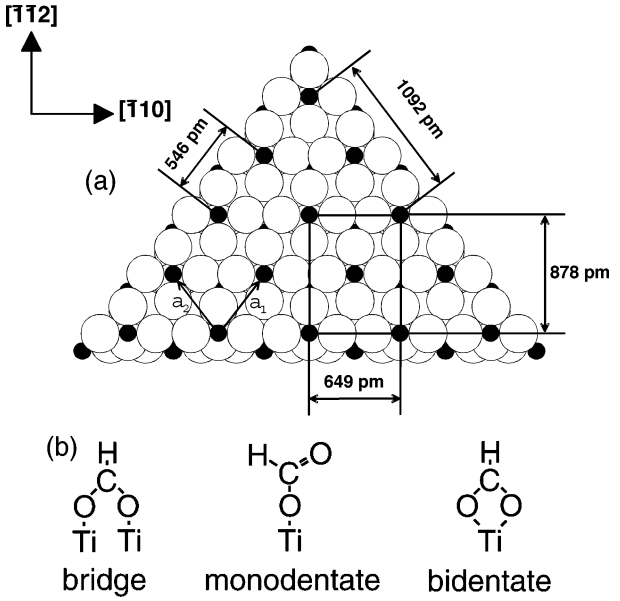

Figure 1. Ideal truncation of a (111) surface of rutile TiO_2. Titanium and oxygen atoms are presented as spheres of their ionic radius in (a). A formate chemisorbed in a monodentate, bidentate, and bridge form is illustrated in (b).

2. Experimental Section

STM and HREELS measurements were done in separate ultrahigh-vacuum chambers. Constant current topography was observed with a scanning tunneling microscope (JEOL, JSPM-4500S) at Kawasaki. A (111)-oriented, one-side-polished wafer ($6.5 \times 1 \times 0.3$ mm^3, Earth Chemicals) was argon ion sputtered at room temperature and vacuum annealed at 970 K. Surface topography was sensitive to the extent of bulk reduction of the crystal.[11] Atomically flat terraces separated by single-height (0.2 nm) steps appeared on a blue wafer prepared with repeated sputter−anneal cycles. Thermal desorption and vibrational spectra were obtained with a similarly prepared TiO_2 surface

† Kanagawa Academy of Science and Technology.
‡ Pacific Northwest National Laboratory.
§ Current address: Technology Research and Development Department, General Technology Division, Central Japan Railway Company, Komaki 485-0801, Japan.
⊥ Current address: Department of Chemistry, Faculty of Science, Kobe University, Kobe 657-8501, Japan.
* To whom correspondence should be addressed. E-mail: oni@kobe-u.ac.jp.

10.1021/jp049126z CCC: $27.50
Published on Web 08/18/2004

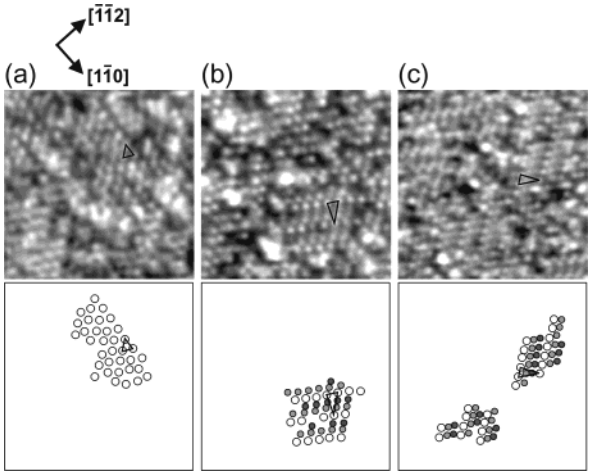

Figure 2. Constant current topography of the sputter-annealed rutile (111) surface. Domains of (1 × 1) symmetry are shown in (a). Image size: 10 × 10 nm^2; sample bias voltage: +0.5 V; tunnel current: 0.1 nA. (1 × 2) domains oriented to the two equivalent directions are in (b) and (c). Image size: 10 × 10 nm^2; sample bias voltage: (b) +0.7 V and (c) +0.5 V; tunnel current: 0.1 nA. Lateral arrangements of topographic protrusions are illustrated in lower panels with different brightness in (b) and (c). One unit cell is superimposed on each panel.

at Richland.[24] Overtones of substrate phonons were Fourier deconvoluted from the loss spectrum collected in the specular scattering direction.[25]

3. Results and Discussion

3.1. STM Topography of the Uncovered TiO_2 (111) Surface. Atom size protrusions were observed on the sputter-annealed TiO_2 surface.[11] Figure 2 shows the protrusions ordered in different symmetries. A fraction of protrusions were aligned on isosceles triangles, the dimension of which (0.6 × 0.6 × 0.7 nm) reproduced the lateral unit cell of Ti atoms expected on the ideal truncation (Figure 1). It is experimentally[8] and theoretically[26] established on the rutile (110) surface positively biased relative to the microscope tip that protrusions in constant current topography represent Ti atoms. The atom size protrusions in Figure 2a were hence assigned to the Ti atoms on the ideal truncation. Another phase of atom arrangement was observed on a major portion of the surface. Bright, less bright, and least bright protrusions appeared, each of which made a row parallel to the two equivalent unit vectors of the ideal truncation, as shown in (b) and (c). The distance between two bright-atom rows was 1.2 nm (twice the unit length in this direction), whereas the atom-to-atom distance along the row axis remained 0.6 nm (the unit length in that direction). This reconstructed phase is indexed as (1 × 2). The order of brightness in the constant current topography reflects the possibility of electron tunnel from the tip, and thus the less bright and least bright atoms are possibly relocated inward relative to the bright atom.

Nanometer-sized domains of (1 × 1) and (1 × 2) phases covered the sputter-annealed surface with disorders at domain edges. Atom vacancies were also present in the domains. The surface of Figure 2 exhibited a (1 × 1) pattern in low-energy electron diffraction though the microscope topography revealed a mixture of (1 × 1) and (1 × 2) patches. Consider the fraction of the two domains. The Ti atom density is 3.5 or 5.3 atoms nm^{-2} in an ideal domain of (1 × 1) or (1 × 2) phase. In the latter phase one protrusion of the three different brightness was counted as one Ti atom. The observed number of protrusions was 4.7 atoms nm^{-2}. (1 × 1) domains and (1 × 2) domains are mixed in a ratio of 1:2 to reproduce the observed number.

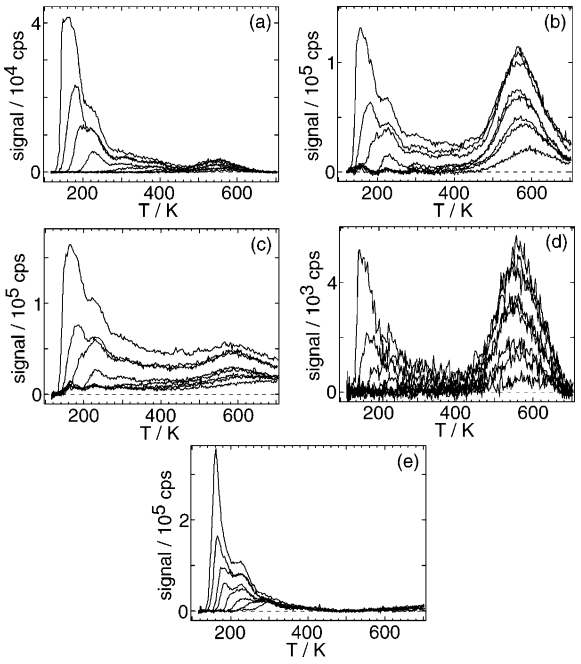

Figure 3. Thermal desorption spectrum of the rutile (111) surface exposed to HCOOH. (a) HCOOH at $m/e = 46$, (b) CO at $m/e = 28$, (c) CO_2 at $m/e = 44$, (d) HCHO at $m/e = 30$, and (e) H_2O at $m/e = 18$. The sputter-annealed surface was exposed to HCOOH at 110 K for 15, 25, 40, 55, 80, 110, 175, and 290 Torr s. The effective pressure was not calibrated on the surface.

3.2. Thermal Desorption Spectrum of Formate-Adsorbed Surfaces. Figure 3 shows a series of desorption spectra observed on the TiO_2 surface exposed to formic acid vapor. The vapor doser was not calibrated, and a relative exposure was given in Torr s based on the pressure measured with a gauge in the gas handling system. Low-temperature desorption of HCOOH appeared at 210 K on the surface exposed to 80 Torr s in Figure 3a and assigned to the desorption of multilayered, physisorbed HCOOH. There were two more desorption regions: one between 300 and 450 K and the other between 450 and 650 K. The former is attributed to the recombination of an adsorbed formate and a proton, whereas the latter is related with decomposition of the formate. Decomposition products (CO, CO_2, and HCHO) were simultaneously released with the high-temperature desorption of HCOOH. The recombination and decomposition reactions occur on rutile (110) at similar temperatures.[27,28] The yield of the decomposition-related peak remained constant at exposures of 100 Torr s or more, suggesting the coverage of the chemisorbed formate was saturated at this exposure. The major product of the formate decomposition was CO with HCHO and CO_2 as shown in panels (b)−(d). Desorption signals below 450 K for these masses were from QMS cracking of formic acid, as can be seen from comparisons with Figure 3a. Molecular hydrogen was not observed. The microscope topography of Figure 2 revealed the heterogeneity of the surface Ti atoms (bright, less bright, and least bright atoms) in addition to vacancies and disorders. Multiple sets of vibrational bands accordingly appeared on the energy-loss spectrum as will be shown in section 3.3. It was, however, difficult to derive the contribution of differently coordinated species from the desorption spectra.

The water desorption spectrum in panel (e) suggests water contamination in our formic acid source. An intense peak existed at 300 K even on the surface of the least exposure. We expect that the contaminated water little affects the observed reactions

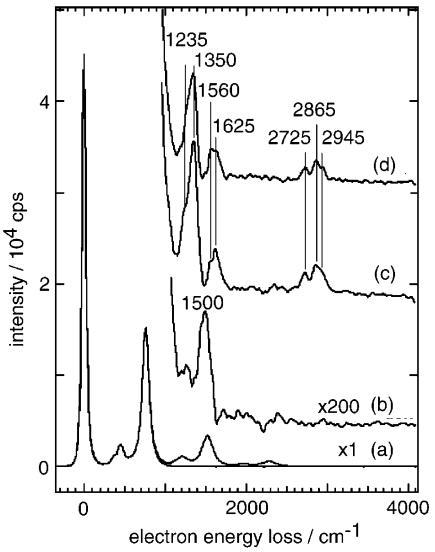

Figure 4. HREEL spectrum of formates chemisorbed on the rutile (111) surface. The raw and Fourier-deconvoluted spectrum of the sputter-annealed surface is shown as (a) and (b). The surface was exposed to formic acid vapor at 120 K and then heated to (c) 350 and (d) 450 K to remove possible contamination of water adsorbed. The spectra were collected at 120 K. The full width of half-maximum of the elastic peak was 56 cm^{-1}.

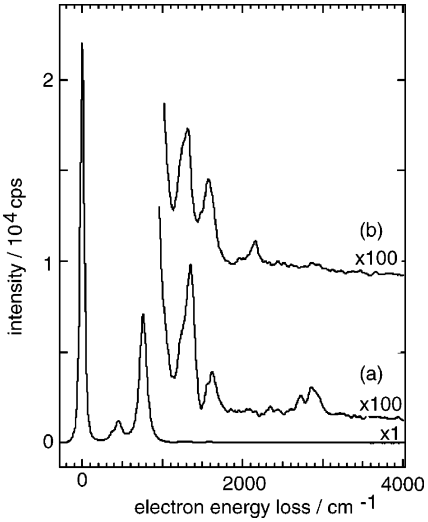

Figure 5. HREEL spectrum of formates chemisorbed on the rutile (111) surface. The sputter-annealed surface was exposed to (a) HCOOH or (b) DCOOD vapor at 120 K and then heated to 350 K. Spectra collected at 120 K were Fourier-deconvoluted. The full width of half-maximum of the elastic peak was 63 cm^{-1}.

of adsorbed formates.[28] The adsorbed water was desorbed when the formate decomposed at 450 K or above.

3.3. Vibrational Spectrum of Adsorbed Formates. The HCOOH-exposed surface was heated at 350 K to remove the possible contamination of adsorbed water before measuring the vibrational spectrum. Figure 4 shows the Fourier-deconvoluted spectrum. Two bands were identified at 2725 and 2865 cm^{-1} with a shoulder peak at 2945 cm^{-1}. The high-wavenumber bands at 2945 and 2865 cm^{-1} are assigned to ν(C−H) of different formate types. If the lowest-wavenumber branch at 2725 cm^{-1} is ν(C−H) of a third formate type, it is from a very weak (acidic) C−H bond. One may alternatively relate that branch to Fermi resonance with the double tone of δ(C−H), the fundamental mode of which is expected around 1300 cm^{-1}. The double tone of symmetry-allowed δ(C−H) is, however, prohibited in dipole scattering.

In the COO-related stretching region, two peaks were resolved at 1350 and 1625 cm^{-1}. Additional peaks can be recognized at 1235 and 1560 cm^{-1}. Those four COO-related bands exhibited no isotope shift on a DCOOD-exposed surface, while the three ν(C−H) bands shifted as expected (Figure 5). The change of the spectrum between 1300 and 1350 cm^{-1} was small in going from HCOOH to DCOOD. The δ(C−H) in this region was weak, if any.

The vibrational spectrum indicated two or more types of formate in accordance with the defects and disorders of the uncovered surface observed by STM. Table 1 presents the wavenumber and assignment of formate-related bands on single-crystalline surfaces of TiO_2 and ZnO. When we assume a bridge formate or a bidentate formate, the two losses at 1350 and 1560 cm^{-1} are ascribed to its symmetric and asymmetric stretching modes, ν_s(O−C−O) and ν_a(O−C−O). The bridge formate on rutile (110) exhibited these modes at corresponding wavenumbers.[17,18] The dipole selection rule of the inelastic electron scattering requires that formate in less than C_{2v} symmetry to give the ν_a(O−C−O) peak of a finite intensity.[29] The bright, less bright, and least bright Ti atoms presented on the (1 × 2) domain can be the reason for the reduced symmetry. The highest wavenumber mode at 1625 cm^{-1} and the lowest wavenumber mode at 1235 cm^{-1} are separated by 390 cm^{-1} and hence attributed to ν(C═O) and ν(C−O) of a monodentate formate. Monodentate formates on a TiO_2 film[30] and ZnO (0001)[31] exhibited ν(C═O) at 1610−1640 cm^{-1}.

One technical issue is noted on the deconvolution of phonons. The deconvoluted spectrum (b) of the clean surface contained a peak at 1500 cm^{-1} (Figure 4). This feature is not due to

TABLE 1: Vibrational Bands of Formate Adsorbed on Single Crystalline Surfaces of Metal Oxide

substrate	method type of formate	wavenumber/cm^{-1} assignment			reference
rutile (110)	HREELS	1365		2920	17
	bridge	ν_s(O−C−O)		ν(C−H)	
rutile (110)	IRAS	1363	1566		18
	bridge	ν_s(O−C−O)	ν_a(O−C−O)		
TiO_2 thin film	HREELS	1355	1637	2928	30
	monodentate	ν(C−O)	ν(C═O)	ν(C−H)	
ZnO (0001)	HREELS	1317	1612	2939	31
	monodentate	ν (C−O)[a]	ν (C═O)[a]	ν(C−H)	
rutile (111)	HREELS	1350	1560	2865	present study
	bidentate or bridge	ν_s(O−C−O)	ν_a(O−C−O)	ν(C−H)	
		1235	1625	2945	
	monodentate	ν(C−O)	ν(C═O)	ν(C−H)	
				2725	
				ν(C−H)?	

[a] Labeled as ν_s(O−C−O) and ν_a(O−C−O) in ref 31.

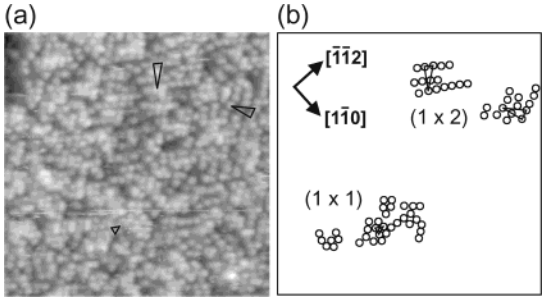

Figure 6. Constant current topography of the formate-covered surface: (a) raw image and (b) an illustration of arrayed protrusions are shown. Image size: 20 × 20 nm^2; sample bias voltage: +1.1 V; tunnel current: 0.4 nA. Unit cells are superimposed.

incomplete removal of the phonon combination peak. Whereas multiple phonon losses arising from multiple dipole losses of a single electron obey Poisson statistics and can be deconvoluted, Wulser and Langell[32] proposed that multiple losses occurring from two different mechanisms (dipole and impact for example) would not be removed by Fourier deconvolution. The absence of this peak on the spectra (c) and (d) of the formate-covered surface evidenced the contribution of impact scattering. The probability of impact scattering is decreased by the presence of a molecular overlayer.

3.4. STM Topography of Adsorbed Formate. Protrusions larger than the Ti atoms were observed on the surface exposed to formic acid vapor at room temperature (Figure 6) and assigned to individual formates chemisorbed on the surface. The lateral distribution of the formates reflected the arrangement of underlying Ti atoms. Formates arrayed on the (1 × 1) and (1 × 2) symmetry were locally recognized as illustrated in (b). This suggests one formate adsorbed on one Ti atom in the arrayed domains. The number density of formate supports the one-to-one relation over the surface. The number of adsorbed formates was 1.9 molecules nm^{-2} in Figure 6 and similarly prepared surfaces. The fraction of (1 × 1) and (1 × 2) domains was estimated to be 1:2 in section 3.1. Here we assume one formate on one Ti atom in the (1 × 1) domain and one formate on one *bright* Ti atom in the (1 × 2) domain. On this assumption, 2.3 formates nm^{-2} is predicted. This number agreed with the observation. The one-to-one adsorption supports the bidentate and monodentate structures among the three types of formate considered in the preceding section.

The lateral mobility of the formate was evaluated on microscope images. Images (a) and (b) of Figure 7 were sequentially recorded at room temperature with a time delay of 189 s. Topographic difference between (a) and (b) determined in

$$z_{\mathrm{diff}}(x,y) = |z_a(x,y) - z_b(x,y)| \qquad (1)$$

is shown as image (c). $z_a(x,y)$ is the topographic height in image (a) at a lateral coordinate (x, y) and so on. Lateral migration of a formate should be recognized in (c) as a pair of bright dots. The result in (c) showed a restricted mobility on rutile (111), not more than 20 movements. Mobility on rutile (110) was evaluated in the same manner. Raw images (d) and (e) were observed on a formate-covered (110) surface maintained at room temperature with a delay of 75 s. Many dot pairs in the image difference (f) indicated frequent migration on the (110) surface. It is known that the Ti atoms separated by 296 pm on this surface allows efficient migration of a formate adsorbed in the bridge form.[33] The limited mobility observed on the (111) surface is interpreted with the monodentate or bidentate form of adsorption. It is difficult for a formate to jump from an adsorption site to another, which are separated by 546 pm or more on the (1 × 1) and (1 × 2) surfaces.

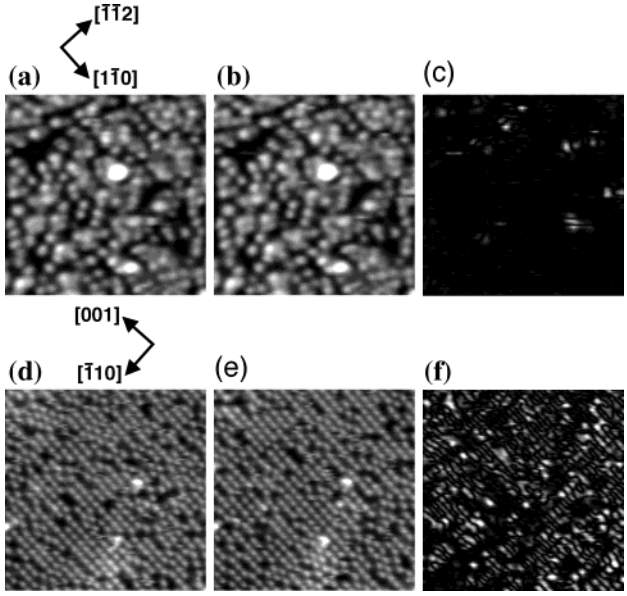

Figure 7. Constant current topography of rutile (111) and (110) surfaces covered with formates. Image (a) and (b) were sequentially obtained on the (111) surface with a time delay of 189 s. Image size: 12 × 12 nm^2; sample bias voltage: +1.4 V; tunnel current: 0.4 nA. Difference between the two is presented in (c). Images (d) and (e) were obtained on a (110) surface with a delay of 75 s. Image size: 16 × 16 nm^2; sample bias voltage: +1.1 V; tunnel current: 0.4 nA. Difference between (d) and (e) is shown in (f).

4. Conclusions

The (111) surface of rutile TiO_2 is covered with nanometer-scale domains of (1 × 1) and (1 × 2) phases when argon ion sputtered and vacuum annealed at 970 K. Formic acid is dissociatively adsorbed on the surface. The recombination and decomposition temperatures of the adsorbed formate are similar to those reported on the (110) surface of this compound. Multiple peaks of the CH- and COO-related stretching modes show two or more types of formate adsorbed at 350 K. The wavenumbers of the stretching vibrations can be interpreted with a mixture of monodentate, bidentate, and bridge adsorption types. The number density and limited mobility of the formates support monodentate and bidentate forms.

Acknowledgment. H.U., A.S., and H.O. acknowledge the support by Core Research for Evolutional Science and Technology of Japan Science and Technology Agency. M.A.H. acknowledges support by the U.S. Department of Energy, Office of Basic Energy Sciences, Division of Materials Sciences. Pacific Northwest National Laboratory is a multiprogram national laboratory operated for the U.S. Department of Energy by the Battelle Memorial Institute under Contract DE-AC06-76RLO1830. A portion of the research reported here was performed in the William R. Wiley Environmental Molecular Science Laboratory, a U.S. Department of Energy user facility funded by the Office of Biological and Environmental Research.

References and Notes

(1) Diebold, U. *Surf. Sci. Rep.* **2003**, *48*, 53.
(2) Cosamdey, F.; Madey, T. E. *Surf. Rev. Lett.* **2001**, *8*, 73.
(3) Sherrill, A. B.; Barteau, M. A. In *Oxide Surfaces*; Woodruff, D. P., Ed.; Elsevier: Amsterdam, 2001; Chapter 10.
(4) Egdell, R. G.; Jones, F. H. *J. Mater. Chem.* **1998**, *8*, 469.
(5) Lai, X.; St. Clair, T. P.; Valden, M.; Goodman, D. W. *Prog. Surf. Sci.* **1998**, *59*, 25.

(6) Bonnell, D. A. *Prog. Surf. Sci.* **1998**, *57*, 187.
(7) Henrich, V. E.; Cox, P. A. *The Surface Science of Metal Oxides*; Cambridge University Press: Cambridge, 1994.
(8) Onishi, H.; Fukui, K.; Iwasawa, Y. *Bull. Chem. Soc. Jpn.* **1995**, *68*, 2447.
(9) Raza, H.; Pang, C. L.; Haycock, S. A.; Thornton, G. *Phys. Rev. Lett.* **1999**, *82*, 5265.
(10) Tero, R.; Fukui, K.; Iwasawa, Y. *J. Phys. Chem. B* **2003**, *107*, 3207.
(11) Uetsuka, H.; Sasahara, A.; Onishi, H. *Jpn. J. Appl. Phys.* **2000**, *39*, 3769.
(12) Tanner, R. E.; Sasahara, A.; Liang, Y.; Altman, E. I.; Onishi, H. *J. Phys. Chem. B* **2002**, *106*, 8211.
(13) Hebenstreit, W.; Ruzycki, N.; Hermanm, G. S.; Gao, Y.; Diebold, U. *Phys. Rev. B* **2000**, *62*, R16334.
(14) Ruzycki, N.; Herman, G. S.; Boatner, L. A.; Diebold, U. *Surf. Sci.* **2003**, *529*, L239.
(15) Onishi, H. In *Chemistry of Nanomolecular Systems*; Nakamura, T., Matsumoto, T., Tada, H., Sugiura, K.-I., Eds.; Springer: Berlin, 2003; Chapter 5.
(16) Thevuthasan, S.; Herman, G. S.; Kim, Y. J.; Chambers, S. A.; Peden, C. H. F.; Wang, Z.; Ynzunza, R. X.; Tober, E. D.; Morais, J.; Fadley, C. S. *Surf. Sci.* **1998**, *401*, 261.
(17) Henderson, M. A. *J. Phys. Chem. B* **1997**, *101*, 221.
(18) Hayden, B. E.; King, A.; Newton, M. A. *J. Phys. Chem. B* **1999**, *103*, 203.
(19) Guo, Q.; Cocks, I.; Williams, E. M. *J. Chem. Phys.* **1997**, *106*, 2924.
(20) Gutiérrez-Sosa, A.; Martínez-Escolano, P.; Raza, H.; Lindsay, R.; Wincott, P. L.; Thornton, G. *Surf. Sci.* **2001**, *471*, 163.
(21) Onishi, H.; Iwasawa, Y. *Chem. Phys. Lett.* **1994**, *226*, 111.
(22) Sasahara, A.; Uetsuka, H.; Onishi, H. *J. Phys. Chem. B* **2001**, *105*, 1.
(23) Käckell, P.; Terakura, K. *Surf. Sci.* **2000**, *461*, 191.
(24) Henderson, M. A. *Surf. Sci.* **1994**, *319*, 315.
(25) Henderson, M. A. *Surf. Sci.* **1996**, *355*, 151.
(26) Diebold, U.; Anderson, J. F.; Ng, K. O.; Vanderbilt, D. *Phys. Rev. Lett.* **1996**, *77*, 1322.
(27) Onishi, H. *J. Catal.* **1994**, *146*, 557.
(28) Henderson, M. A. *J. Phys. Chem.* **1995**, *99*, 15253.
(29) Sexton, B. A. *Surf. Sci.* **1979**, *88*, 319.
(30) Chang, Z.; Thornton, G. *Surf. Sci.* **2000**, *462*, 68.
(31) Petrie, W.; Vohs, J. M. *Surf. Sci.* **1991**, *245*, 315.
(32) Wulser, K. W.; Langell, M. A. *Phys. Rev. B* **1993**, *48*, 9006.
(33) Onishi, H.; Iwasawa, Y. *Langmuir* **1994**, *10*, 4414.